

Research paper

Effects of erosion on the microaggregate organic carbon dynamics in a small catchment of the Loess Plateau, China



Yixia Wang^{a,b}, Nufang Fang^a, Fengbao Zhang^a, Ling Wang^{a,b}, Gaolin Wu^a, Mingyi Yang^{a,*}

^a State Key Laboratory of Soil Erosion and Dryland Farming on the Loess Plateau, Institute of Soil and Water Conservation, Chinese Academy of Sciences and Ministry of Water Resources, Yangling, Shaanxi Province, 712100, PR China

^b University of Chinese Academy of Sciences, Beijing 100049, PR China

ARTICLE INFO

Keywords:

Check dam
Sediment
Soil erosion
Microaggregate
Organic carbon

ABSTRACT

Soil erosion significantly affects the dynamics of the terrestrial carbon (C) cycle. Erosion removes C-rich topsoil and deposits it in lower-elevation areas and exposes deeper C-poor horizons at the surface. However, the mechanisms responsible for the mobilization and deposition of microaggregate soil organic carbon (SOC) due to soil erosion at the catchment scale remain unclear. The main objective of this study is to illustrate the effects of different erosion processes on the distribution and deposition of microaggregate SOC. The activity of ¹³⁷Cs and extreme rainfall events were used as dating methods. Based on the microaggregate size distribution and the K-means clustering approach, 75 flood couplets were identified in an 11.3-m sediment deposit profile of the check dam in the Nianyangou catchment and classified into three couplet types. In each flood couplet, the SOC concentrations and amounts in three microaggregate fractions (250–50, 50–20 and < 20 μm) were quantified. The following results were obtained. (1) ¹³⁷Cs activity and a record of extreme rainfall events can be used to characterize the sediment deposition process. (2) Sediments with fine microaggregate fractions (Couplet Type I) contained abundant SOC and were mainly associated with low-intensity rainfall conditions, whereas sediments with coarse microaggregate fractions (Couplet Type III) had higher SOC concentrations and were mainly associated with high-intensity rainfall conditions. (3) Couplet Type I sediments were most likely related to sheet and interrill erosion, whereas Couplet Type III sediments were likely associated with rill and gully erosion. Our study contributes to the understanding of the effects of soil erosion on microaggregate SOC dynamics at the catchment scale and further illustrates the carbon sequestration mechanism active in check dams of the Loess Plateau.

1. Introduction

The biogeochemical cycle of carbon (C) in terrestrial ecosystems has received increasing attention worldwide recent decades because of the emission of carbon dioxide (CO₂) into the atmosphere (Fu et al., 2010). Soil C is a critical component of the C cycle and is two times more abundant than atmospheric C and three times more abundant than vegetation C; thus, it accounts for approximately two-thirds to three-fourths of the terrestrial C pool (Smith et al., 2008). Soil organic carbon (SOC), an active component of the soil C pool, has received substantial attention in the field of global change research (Lü et al., 2012). Soil erosion and deposition have been reported to strongly affect the soil C pool of a catchment by removing SOC-rich topsoil, depositing it in low-lying depositional environments (Berhe et al., 2007; Lal, 2003; Starr et al., 2000), and exposing SOC-poor subsoil at the surface. Therefore,

elucidating the dynamics of the SOC retained in sediments affected by soil erosion and deposition is necessary to understand the important role of soil erosion in the terrestrial C cycle (Berhe et al., 2007; Harden et al., 1999; Van Oost et al., 2007).

Soil erosion is a complex process (Gregorich et al., 1998) that causes transport and deposition of sediment with accompanying SOC (Wang et al., 2014a, 2014b). Previous studies have revealed that different erosion processes lead to different sediment SOC concentrations through selective particle size mobilization (Nadeu et al., 2011). For instance, sheet and interrill erosion selectively remove fine particles from SOC-rich topsoil, whereas rill and gully erosion are less selective (or non-selective) and mobilize large amounts of sediment from the topsoil and deeper horizons (Durnford and King, 1993; Issa et al., 2006). Consequently, erosion processes that affect only topsoil will result in relatively high SOC values, as found for sheet and interrill

Abbreviations: C, carbon; SOC, soil organic carbon; TOC, total organic carbon

* Corresponding author.

E-mail addresses: wuyixia@126.com (Y. Wang), fnf@ms.iswc.ac.cn (N. Fang), fbzhang@nwsuaf.edu.cn (F. Zhang), wangling_ln@126.com (L. Wang), gaolinwu@gmail.com (G. Wu), myzyly@163.com (M. Yang).

<http://dx.doi.org/10.1016/j.still.2017.08.001>

Received 17 June 2016; Received in revised form 1 August 2017; Accepted 2 August 2017
0167-1987/ © 2017 Elsevier B.V. All rights reserved.

erosion (Schiettecatte et al., 2008). In contrast, lower SOC values are expected in eroded sediments resulting from rill and gully erosion (Schiettecatte et al., 2008). These erosion processes are characterized by their aggregate size distributions, which provide information on erosion mechanisms and the depositional size selectivity (Slattery and Burt, 1997). Additionally, these distributions have been used to assess the types of processes resulting in sediment deposition (Beuselink et al., 2000). Soil aggregates physically protect SOC from rapid decomposition by soil microbes (Razafimbelo et al., 2008; Six et al., 2000), and aggregate formation appears to be closely linked to soil carbon storage and stability (Barreto et al., 2009; Golchin et al., 1995; Salomé et al., 2010). A study conducted by Six et al. (2004) confirmed that the turnover time of macroaggregates is shorter than that of microaggregates; thus, microaggregates are more important for the physical protection of SOC. Although macroaggregates allow greater SOC storage, this storage is temporary; in contrast, microaggregates promote the long-term fixation of SOC. However, the reported relationships between SOC and sediments have mainly focused on dispersed particle distributions and overlooked the implications of how clay is transported. The transport form of clay fraction is dispersed or within aggregates, which is critical to assessing the fate of SOC (Nadeu et al., 2011).

The Loess Plateau of China is internationally recognized as suffering from severe soil erosion (Fu et al., 2011). Over 60% of the land area is susceptible to soil and water losses, and the soil in this region is the “most highly erodible soil on earth” (Lafren and Tian, 2000). Soil conservation measures are needed to control soil and water losses and improve productivity levels. Approximately 110,000 check dams have been constructed in the Loess Plateau region and now store $21 \times 10^9 \text{ m}^3$ of sediment and 0.0952 Gt ($1 \text{ Gt} = 10^9 \text{ Mg} = 10^{15} \text{ g}$) of SOC (Wang et al., 2011, 2014c). The sediments deposited behind the check dams, are believed to protect SOC from decomposition by creating unfavourable conditions for SOC mineralization (increased wetness and reduced oxygen) (Berhe et al., 2007; Harden et al., 1999; Stallard, 1998). Thus, the sediments retained by the check dam play a significant role in carbon sequestration in the agro-ecosystems of the Loess Plateau (Cao et al., 2009, 2010; Yang et al., 2010). In addition, the sediments exhibit a clear sedimentary sequence, with the thickness of each couplet varying from a few centimetres to several decimetres (Chen et al., 2016). The different thicknesses of the sediment couplets reflect the degree of rainfall erosion intensity (Yang et al., 2006; Zhang et al., 2006). Such situations provide ready access to flood couplet records, without the need for laborious excavation or coring. The relationship between sediments and evolution of the environment has

been mainly studied in reference to lacustrine, littoral, and sublittoral habitats (Girardclos et al., 2005; Jennings et al., 2001; Wasson et al., 2002), and high-resolution results based on the sediments in these depositional sites are lacking.

Sediments trapped by check dams can serve as natural archives for reconstructing the environmental history of soil erosion in a small catchment (Dearing et al., 2001, 2008; Sritrairat et al., 2012). These sediments have great potential for high-resolution environmental change research based on soil erosion in the hilly Loess Plateau. The main objectives of this study are as follows: (1) to quantify distributions of different microaggregate fractions (250–50, 50–20 and $< 20 \mu\text{m}$) and the accompanying SOC dynamics of each flood couplet and (2) to further clarify the relationship between microaggregate SOC transport and related erosive rainfall events and thereby reveal the effects of different erosion processes on the distribution of microaggregate SOC. Based on the results, we can elucidate the effects of accelerated erosion on SOC storage in check dams of the Loess Plateau.

2. Study area and methods

2.1. Study area

This study was conducted in the Nianyangou catchment ($37^{\circ}35'33''\text{N}$ to $37^{\circ}35'54''\text{N}$, $110^{\circ}22'4''\text{E}$ to $110^{\circ}22'28''\text{E}$), which is located in Suide County, Shaanxi Province, on the Loess Plateau. The elevation within the catchment ranges from 1027 m to 1118 m, and the slope gradient ranges from 0 to 19.7° , with an average value of 12.5° . Areas in which gradients exceed 10° constitute 49.2% of this catchment. The drainage basin is characterized by terrain fragmentation and complex topography. The soil is mainly derived from loess formations with textures ranging from fine silt to silt, and it is vulnerable to erosion (Fu et al., 2000). The catchment experiences a temperate continental monsoon climate with a mean annual precipitation level of 513 mm, of which more than 70% falls in the rainy season (June to September), primarily in the form of high-intensity rainstorms (Yang et al., 2006).

The sampling area, a check dam in the Nianyangou catchment, has a well-documented history. It was constructed in the catchment in 1960 and had completely filled with sediment by 1990. This check dam controls an area of approximately 18.1 ha, and the silted-in area currently covers approximately 6000 m^2 (Fig. 1). High-precision global positioning system (GPS) data combined with QuickBird imagery were used to create a topographic catchment map (1:10,000 scale). During the check dam siltation period, land use in the catchment was mainly characterized by sloping cropland which covered 77.2% of the

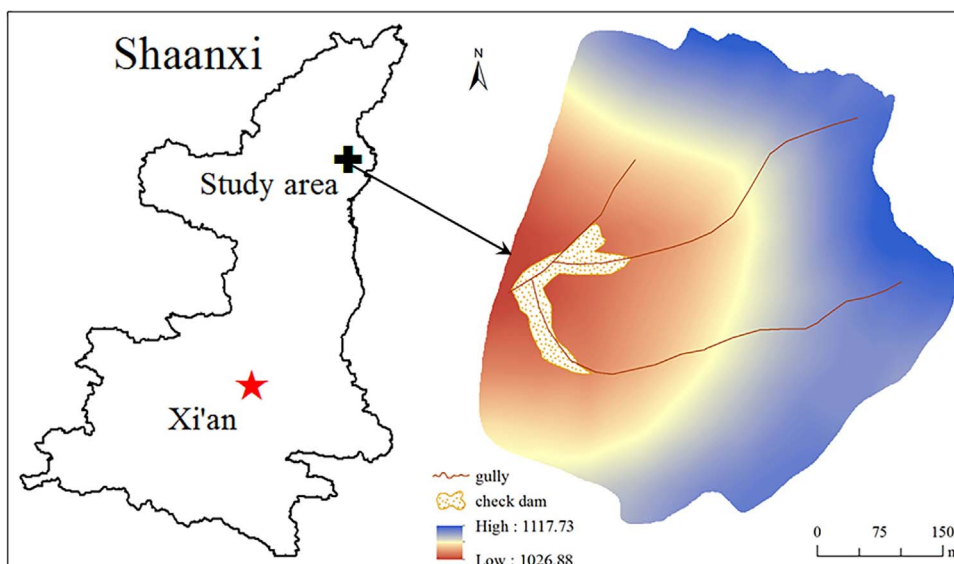


Fig 1. Location of the study area.

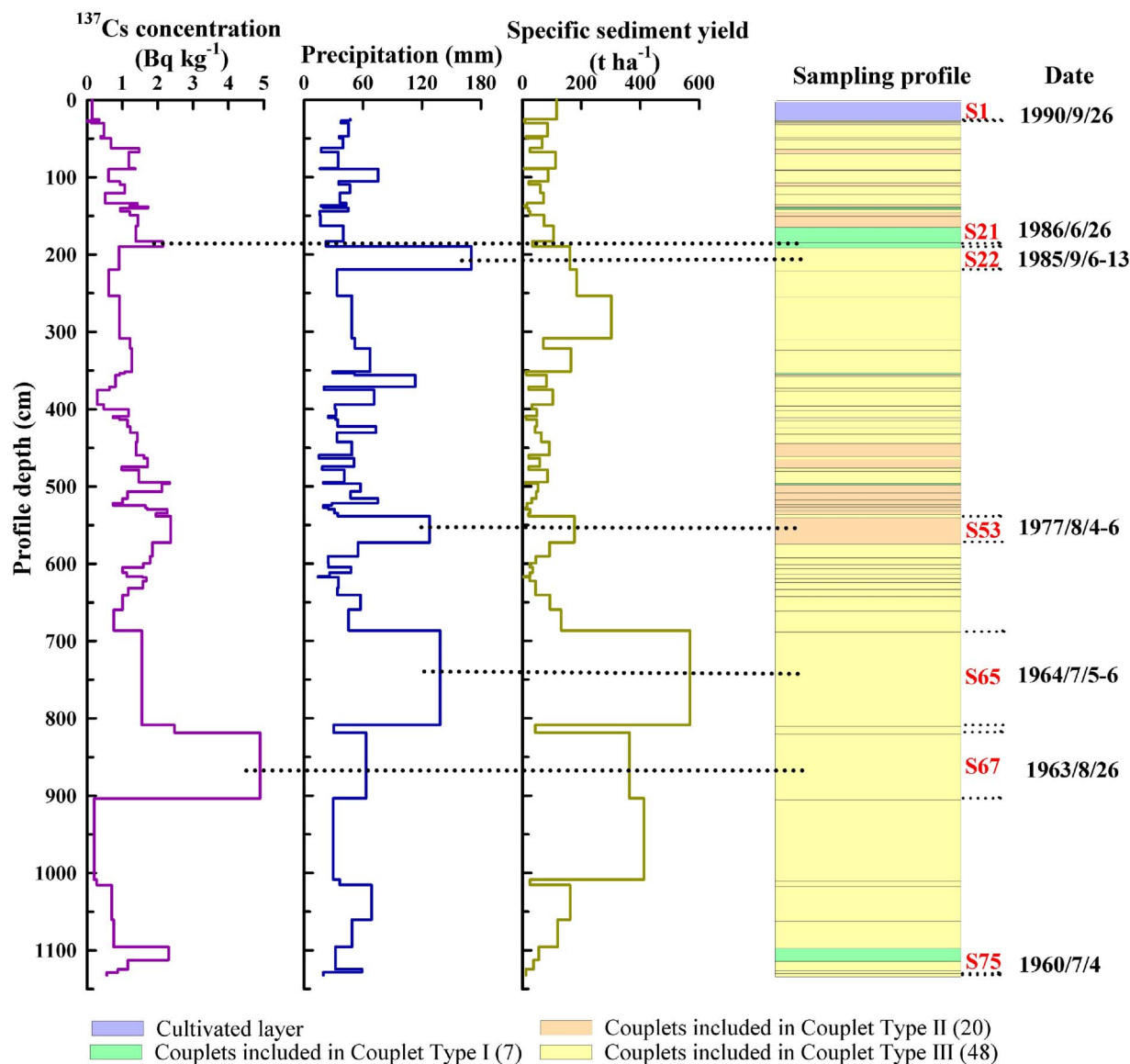


Fig. 2. Depth distributions of ¹³⁷Cs, rainfall precipitation and specific sediment yield in the deposit profile. Figures in brackets refer to the number of couplets in the respective couplet type. The dotted line denotes the layer between the ¹³⁷Cs distributions and the sampling profile or between the rainfall precipitation and the sampling profile.

catchment area, and only a small fraction of the land was occupied by shrubs, which were mainly located on gullies.

2.2. Sediment sample collection

Sediment samples were collected for analysis in September 2009. We selected a sediment deposit profile with a height of 11.3 m and carefully sectioned it to identify the flood couplets. The sediment profile was undisturbed, as indicated by the clear water-sediment interface and preserved fine sediment laminations. The boundaries between couplets associated with individual floods were easily defined because each couplet featured a bottom layer composed of coarse sediment and an upper layer composed of fine sediment (Wang et al., 2014b). The thickness of each couplet was measured in situ, and the thicknesses varied from 1 cm to 122 cm (Fig. 2). We collected 76 sediment samples from the deposit profile, obtaining the first sample from the cultivated layer (Fig. 2). In addition, 10 randomly selected undisturbed sediment samples (rings of 100 cm³) along the deposit profile were collected to estimate bulk density.

2.3. Sediment volume and sediment yield estimation

We estimated the capacity curve of the check dam using the “3D Analyst Tool” in ArcGIS10.1 combined with the depth and sedimentary thickness. According to the 10 measured values of bulk density determined from the randomly selected undisturbed sediment samples, we calculated the simulation curve of the bulk density (Eq. (1)) of the check dam (Xue et al., 2011). The capacity curve of the check dam (Eq. (2)) illustrates the relationship between the accumulative reservoir storage capacity and the depth. Using Eqs. (1) and (2), we determined the sediment yield of each sediment couplet and the total sediment yield of the check dam (Table S1).

$$BD = 0.1409\ln(D) + 0.7068, \quad R^2 = 0.9918 \quad (1)$$

$$ASV = 0.0167(D)^2 - 75.563(D) + 63959, \quad R^2 = 0.9999 \quad (2)$$

The parameters *BD*, *D* and *ASV* refer to the bulk density (g cm⁻³), depth (cm), and accumulative sediment volume (m³), respectively.

2.4. Laboratory analysis

The collected sediment samples were sealed in clean plastic bags and transported to the laboratory. The samples were air-dried for approximately 3 days in a dry and well-ventilated room until a constant weight was reached. All of the samples were dry-sieved through a 2-mm sieve to remove stones, roots, and other debris before conducting ^{137}Cs activity and microaggregate fractionation analyses. ^{137}Cs activity levels were determined via gamma spectrometry using a hyperpure coaxial germanium detector connected to a multi-channel digital analyser system (ORTEC, Oak Ridge, Tennessee, United States). All of the sample weights exceeded 300 g, and ^{137}Cs was measured at 661.6 keV with a counting time of $\geq 28,800$ s (Xue et al., 2011; Zhao et al., 2015).

The distribution of microaggregates in the 2-mm sieved, air-dried samples was determined via a pipette method adapted from Liu et al. (1996). Ten grams of soil was rapidly immersed in 150 mL of deionized water in a 250 mL plastic bottle for 24 h, and the bottle was then subjected to a reciprocal shaker oscillation for 2 h. The contents of the bottle were then passed through a 250 μm sieve to a 1 L glass sedimentation cylinder. Due to the soil texture, all of the fractions passed through the 250 μm sieve. We then used a stirring rod to mix the suspension for 1 min while ensuring vertical motion (up and down 30 times), and each suspension was left to stand for the appropriate settling time for the < 50 or < 20 μm fraction. Aliquots of the < 50 and < 20 μm fractions were siphoned from the upper 13 cm of the suspensions and into beakers with known and constant weights. We then dried the beakers to a constant weight at 60–70 °C and determined the microaggregate fraction (< 50 and < 20 μm) contents relative to the cylinder volume. The content of the 50–20 μm fraction was calculated based on the difference between the < 50 and < 20 μm fractions, and the content of the 250–50 μm fraction was determined based on the difference between the total soil and the < 50 μm fraction. Three replicates per sample were analysed. The traditional pipette method depends on the physical fractionation of the soil based on the soil particle sizes, which affect subsequent SOC analyses less significantly than alternative methods, such as dry-sieving, ultrasonication or chemical dispersion (Saviozzi et al., 1997; Stemmer et al., 1998).

To measure the total organic carbon (TOC) concentration, an air-dried, undisturbed sub-sample from each sediment layer, was ground to pass through a 0.25-mm sieve. The SOC concentrations of the total soil and microaggregate fractions (< 50 and < 20 μm) were analysed using a VARIO EL III CHON elemental analyser (Elementar, Germany) at the Testing and Analysis Center of Northwest University, China. Prior to the analysis, carbonates were removed from the samples using hydrochloric acid. The relative SOC amount in each microaggregate was calculated by multiplying the SOC concentration per size fraction by the mass of microaggregates per fraction. The SOC amounts of 250–50 and 50–20 μm fractions were calculated based on the difference between the total soil and < 50 μm fraction and the difference between the < 50 and < 20 μm fractions, respectively. The SOC concentrations of the 250–50 and 50–20 μm fractions were determined by dividing the SOC amount by the content of each fraction.

2.5. Statistical analysis

A clustering approach was used to classify the flood couplets into different types according to the mass fractions of the different microaggregate fractions. The clustering approach has been widely used in various scientific fields (Anderberg, 1988; Yeh et al., 2000), especially in classifying numerous rainfall events into different groups for statistical analysis (Fang et al., 2012; Peng and Wang, 2012). There are two methods of clustering, the hierarchical clustering method and the non-hierarchical method, i.e., K-means clustering. The K-means clustering method was applied to this study. This method is suited to a large number of cases (Hong, 2003), and a cluster number is required before classification. To determine the number of clusters in a dataset,

numerous criteria have been proposed (Perruchet, 1983). In our study, the most suitable clusters were chosen by trial and error. The classifications satisfied the analysis of variance (ANOVA) significance criterion ($p < 0.001$).

All statistical, cluster and variance analyses were performed using SPSS (version 18.0) for Windows. A one-way ANOVA conducted via Tukey's test and a mean comparison according to the lowest significance level were used for multiple comparisons of the examined rainfall, sediment and organic carbon variables among the different couplet types.

3. Results

3.1. Characteristics of the deposit profile and related historical rainfall events

According to the sediment particle size distribution, 76 couplets (1 cultivated layer and 75 flood couplets) were identified in the 11.3-m profile. The field survey suggested that the check dam began to accumulate silt from 1960 and had become completely filled by 1990. Consequently, the top couplet in the profile had developed by approximately 1990, and the bottom couplet developed in approximately 1960 (without considering the upper cultivated layer, Fig. 2).

The ^{137}Cs activity profile distribution (Fig. 2) includes two peaks (4.898 Bq kg^{-1} in S67 and 2.149 Bq kg^{-1} in S21). These two values reflect a period of global fallout in the northern hemisphere associated with weapons testing in 1963 (Collins et al., 1997; Ritchie and McHenry, 1990; Walling and He 1997) and the Chernobyl-associated tertiary peak in 1986 (Klaminder et al., 2012), respectively. Thus, the corresponding flood couplets can be dated to rainstorms in 1963 and 1986. A study conducted by Xie et al. (2000) showed that precipitation levels exceeding 12 mm can be erosive on the Loess Plateau. Accordingly, 75 related erosive rainstorms were identified in the 11.3-m profile (Table S1). The rain storm parameters, sediment volume, sediment yield and specific sediment yield for each couplet are shown in Table S1. Couplets related to extreme floods with high specific sediment yields formed in 1963 (S67), 1964 (S65), 1977 (S53) and 1985 (S22) (Fig. 2). Relatively small flood couplets were identified between these large floods.

This dating provided a good opportunity for identifying other flood events. Among the 75 sediment couplets, two couplets, i.e., S65 and S68, were > 100 cm in thickness and correspond to the largest floods (Table S1). The sediment volume (yield) was positively correlated with precipitation and maximum 60-min rainfall intensity (I_{60}) at the $p < 0.0001$ level. The sediment yields of S65 and S68 were more than 7000 t and were related to the high values of precipitation (138.4 mm) and I_{60} (0.85 mm min^{-1}). Furthermore, the specific sediment yields of S65 and S68 were estimated to be 568.5 and 412.8 t ha^{-1} , respectively. The wettest year was 1963, which featured two extreme rainfall events (6/15/1963 and 8/26/1963), whereas no floods occurred in 1965. The annual sediment yields varied from 0 in 1965 to 1.5×10^4 t in 1963, and the total value of the sediment trapped by the check dam was 9.9×10^4 t.

3.2. Couplet classifications and types corresponding to rainfall events

The profile distributions of the mass fractions of the microaggregates fractions (250–50, 50–20 and < 20 μm) are shown in Fig. 3. The mass fractions of 250–50, 50–20 and < 20 μm fractions were 54–381 g kg^{-1} , 289–693 g kg^{-1} and 96–560 g kg^{-1} , respectively, with means of 239 g kg^{-1} , 541 g kg^{-1} and 219 g kg^{-1} , respectively. The 75 flood couplets were divided into three types via K-means clustering and were named Couplet Type I, Couplet Type II and Couplet Type III (Table 1 and Fig. 2).

The mean mass of the < 20 μm microaggregate fraction decreased in the following order: Type I $>$ Type II $>$ Type III, while that of the

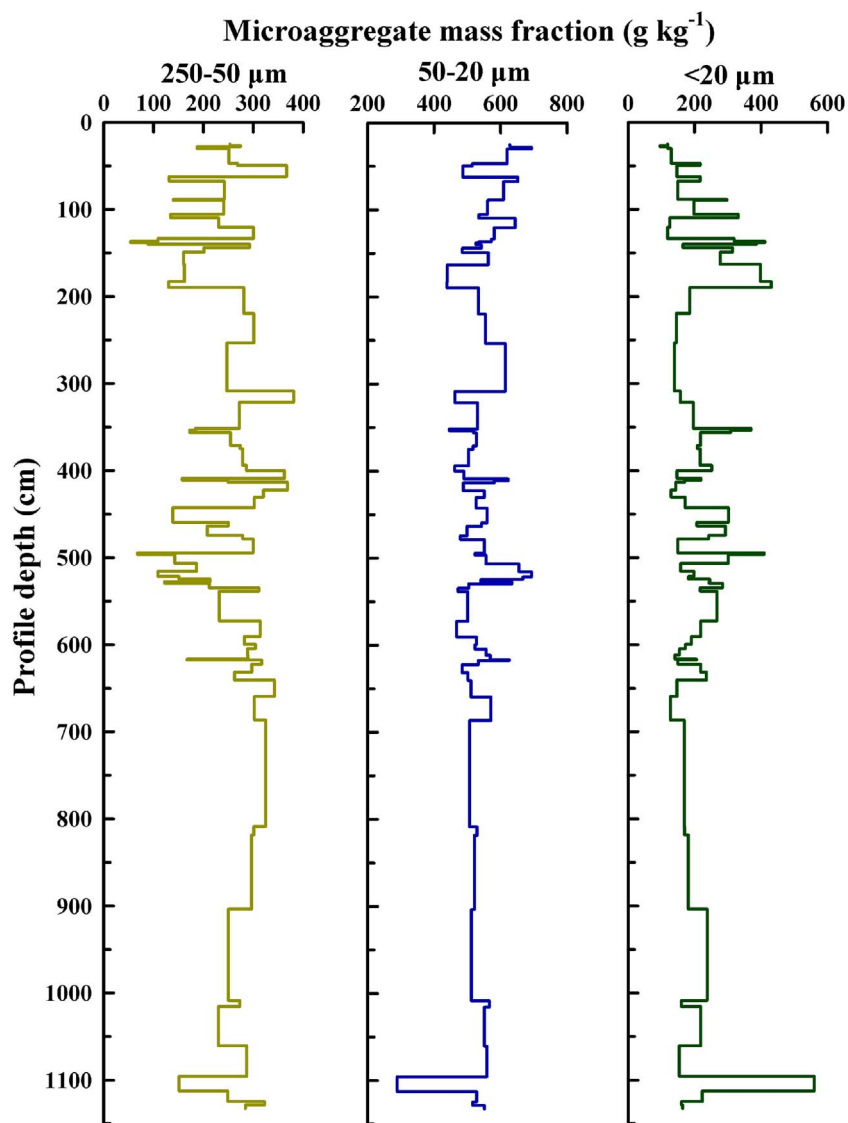


Fig. 3. Sediment microaggregate size distribution in the deposit profile.

Table 1
Statistical features of different couplet types.

Couplet Type	Microaggregate size (μm)	Mean mass fraction (g kg ⁻¹)	Standard deviation	Variation coefficient (%)	Couplet number
I	250–50	119.7	50.16	41.91	7
	50–20	456.4	85.74	18.79	
	< 20	423.9	63.08	14.88	
II	250–50	163.7	36.61	22.37	20
	50–20	582.0	67.90	11.67	
	< 20	254.3	59.36	23.34	
III	250–50	288.6	36.14	12.52	48
	50–20	537.2	45.16	8.41	
	< 20	174.2	38.18	21.91	

250–50 μm fraction exhibited the opposite trend. For the 50–20 μm microaggregate fraction, Type II had the highest mean values, followed by Types III and I. The general characteristics of each Couplet Type are as follows: Couplet Type I includes couplets with the finest microaggregates, whereas Couplet Type III includes couplets with the coarsest microaggregates. Couplet Type II comprises moderately sized microaggregates and features the highest mean mass value of the 50–20 μm microaggregate fraction (Table 1, Fig. 4c).

Among the 75 couplets examined, 48 couplets were classified as Type III, with a total sediment volume of 52,239 m³ and a total sediment yield of 80,910 t (Table 2). Additionally, 20 couplets were classified as Type II, with a total sediment volume and sediment yield of 8698 m³ and 13,305 t, respectively. However, only 7 couplets were classified as Type I, with a total sediment volume of 2851 m³ and a total sediment yield of 4282 t. Type III presented the highest sediment volume and yield and was significantly larger than Types II and I, whereas no significant difference was found between Types II and I (Table 2).

Table 3 shows the rainfall events corresponding to the three couplet types. The values of accumulated rainfall precipitation (AP) and duration (AD) of Types II and III were much higher than those of Type I. Type III exhibited the highest values of mean rainfall precipitation (MP) and mean maximum 60-min intensity (MI₆₀), whereas the mean rainfall duration (MD) for Type III was slightly smaller than that of Type II. The MP values of Types I and III were significantly different (*p* < 0.05), whereas the values of MD and MI₆₀ were not significantly different among the three types. The main eigenvalues of related rainstorms were different among the three types, especially the value of MP.

3.3. Microaggregate SOC in different couplet types

The average SOC concentrations and SOC amounts of different microaggregate fractions in different couplet types are shown in Fig. 4.

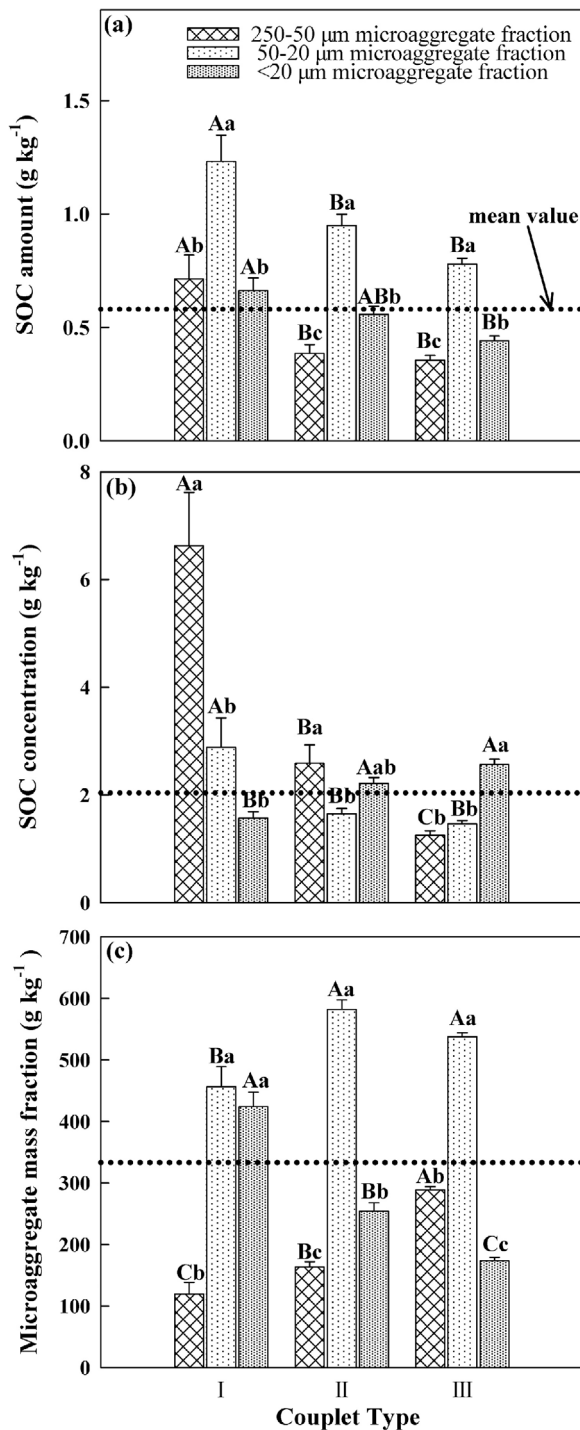


Fig. 4. SOC amount (a), SOC concentration (b) and mass fraction (c) for each microaggregate fraction of the different couplet types. The values for the same microaggregate size in different couplet types followed by the same uppercase letter and the values for different microaggregate sizes of one couplet type followed by the same lowercase letter are not significantly different at $p < 0.05$. Values are means \pm stand errors. The dashed line in this figure denotes the mean value.

The average SOC concentrations of the 250–50 μm and 50–20 μm microaggregate fractions of the different couplet types exhibited the following order: Type I > Type II > Type III (Fig. 4b). In contrast, Type III had the highest mean SOC concentration for the < 20 μm fraction, followed by Types II and I. Decreasing trends in the average SOC amount were found for all three microaggregate fractions (Fig. 4a). The 50–20 μm fraction contained the highest mean amount of SOC in all three couplet types (Fig. 4a). For Types II and III, the < 20 μm fraction

Table 2
Main statistical features of flood couplets for different couplet types.

Couplet Type	Main statistical features				
	N	TSV (m ³)	TSY (t)	¹ Log (MSV)	¹ Log (MSY)
I	7	2851	4282	2.41 b	2.58 b
II	20	8698	13305	2.46 b	2.63 b
III	48	50418	78798	2.80 a	2.99 a

Note: N, the number of couplets in each couplet type; TSV, total sediment volume; TSY, total sediment yield; MSV, mean sediment volume; MSY, mean sediment yield.

* Different letter designations indicate significant difference at $p < 0.05$; to satisfy the Test of Homogeneity of Variances requirements, data were analysed via logarithmic transformation.

Table 3
Main eigenvalues of related rainfall storms for different couplet types.

Couplet Type	Main rainfall eigenvalues					
	N	AP (mm)	AD (min)	MD (min)	M_{I60} (mm min ⁻¹)	¹ Log(MP)
I	7	179.8	4084	583	0.23	1.39 b
II	20	783.4	20966	1103	0.24	1.52 ab
III	48	2277.8	44343	1031	0.29	1.62 a

Note: N, the number of related rainfall storms for each couplet type; AP, accumulated rainfall precipitation; AD, accumulated rainfall duration; MD, mean rainfall duration; MP, mean rainfall precipitation; M_{I60} , mean maximum 60-min rainfall intensity.

* Different letter designations indicate significant difference at $p < 0.05$; to satisfy the Test of Homogeneity of Variances requirements, data were analysed via logarithmic transformation.

had the second highest mean SOC amount, and the 250–50 μm fraction had the lowest mean SOC amount. However, in Type I, the average SOC amount in the 250-50-μm fraction was higher than that in the < 20 μm fraction.

The amount of TOC in the eroded sediments was estimated to be 172.6 t over a 30-year period, and the specific eroded SOC yield was 9.5 t ha⁻¹. The microaggregates of the 250-50, 50-20 and < 20 μm fractions contained 39.0 t, 85.2 t and 48.5 t, respectively, and accounted for 22.6%, 49.4% and 28.1% of the TOC amount, respectively. The distribution of eroded SOC varied among the three couplet types. In Type I, which was related to 7 erosive rainfall events, the TOC amount was 14.3 t, which was equivalent to a production of 2.0 t in each event. For Type II, which corresponded to 20 erosive rainfall events that produced 28.2 t of eroded SOC, the average erosion rate of each rainfall event was 1.4 t. The TOC amount produced by Type III (48 rainfall events) was 130.1 t, and each event transported approximately 2.7 t of eroded SOC.

Our correlation analysis revealed that TOC levels in sediments under different couplet types were related to the mass fraction, SOC concentration and amount of different aggregate size fractions (Table 4). Overall, TOC was negatively correlated with coarser mass fractions (250–50 μm and 50–20 μm) and positively correlated with the finer mass fraction (< 20 μm), especially the significant correlation in Type I. For all 75 sediment samples in the profile, the TOC correlated positively with SOC concentration and amount in all microaggregate fractions, especially the 50–20 μm fraction.

4. Discussion

4.1. Effects of soil erosion on sediment aggregate size distribution and deposition

Check dam sediments may serve as an important indicator for reconstructing the environmental history of soil erosion in a given location (Wang et al., 2014b). Our findings indicate that sediment

Table 4
Pearson correlation coefficients between TOC and the studied microaggregate variables of different couplet types.

TOC	Microaggregate mass fraction			Microaggregate SOC concentration			Microaggregate SOC amount		
	250–50 μm	50–20 μm	< 20 μm	250–50 μm	50–20 μm	< 20 μm	250–50 μm	50–20 μm	< 20 μm
^a I	–0.108	–0.777*	0.970**	0.370	0.985**	0.020	0.753	0.858*	0.643
^a II	–0.349	–0.167	0.406	0.573**	0.623**	0.489**	0.547**	0.646**	0.740**
^a III	–0.059	–0.189	0.279	0.526**	0.694**	0.432**	0.540**	0.738**	0.566**

*and ** donate significance at $p < 0.05$ and 0.01 , respectively.

^a I, II and III refer to Couplet Type I, Couplet Type II and Couplet Type III, respectively.

aggregate size distributions are strongly affected by soil erosion. In this intensively cultivated catchment, the sediments are sorted by each erosive rainfall event in the upstream watershed then deposit behind the check dam. Therefore the sediments can be correlated with different erosion processes in the upstream watershed.

In this study, the sediment size distribution changed significantly among the three couplet types ($p < 0.05$) (Fig. 4). However, this result could not be explained by particle size differences in the original soils because the sediments of the three couplet types came from the same original soils. In addition, although the sedimentary periods of each flood couplet varied substantially, sediment deposition processes exerted limited effects on the aggregation of different size fractions because of the less-favourable conditions of soil microbial activity (Berhe et al., 2007; Wang et al., 2014a). Consequently, we conclude that different erosion processes affect the sediment size distribution and deposition (Panuska et al., 2008; Rose et al., 2007; Shi et al., 2013). Previous studies have shown that sheet and interrill erosion selectively remove fine particles, whereas rill and gully erosion are less selective, mobilizing large amounts of coarse particles (Durnford and King, 1993; Issa et al., 2006). Therefore, we speculate that the most relevant erosion process of Couplet Type I is sheet and interrill erosion because of the sediments are predominantly fine (< 20 μm). In contrast, the sediments in Couplet Type III contain coarse (250–50 μm) components and are probably related to rill and gully erosion. Couplet Type III included 48 flood couplets accounting for 64% of the total. Consequently, in this intensively cultivated catchment, the dominant erosion processes were rill and gully erosion, which were also the primary erosion processes found in the Loess Plateau gully area (Wang et al., 2014b).

The varying flow transport capacities contributed to the different levels of selectivity between the two erosion processes (Nadeu et al., 2011; Shi et al., 2012). The transport of sediment particles in the form of large aggregates or coarse fractions requires high flow transport capacity levels (Nadeu et al., 2011). Therefore, rainfall events characterized by large precipitation amounts, long durations and/or high rainfall intensities generate high flow transport capacity levels (e.g., the rainfall characteristics associated with Couplet Type III). The 250–50 μm microaggregate fraction exhibited the lowest mass fraction among the three size fractions in Couplet Types I and II (Fig. 4c). These results are mainly attributable to the presence of lower transport forces than those of Type III. Indeed, in this case, the forces were not sufficient to carry sand-sized particles and/or disintegrate many large aggregates during transport. In contrast, the sediments in Type III contained the fine sand size fraction (250–50 μm) due to large rainfall amounts and high rainfall intensities.

4.2. Relationship between SOC and microaggrete size distribution

Palis et al. (1990) noted that nutrient and carbon distributions are non-uniform over different size fractions of sediment particles: fine sediments are usually richer in nutrients and carbon than coarse sediments. In this study, the 250–50, 50–20 and < 20 μm microaggregate fractions contained 22.6, 49.4 and 28.1% TOC on average, respectively. A similar trend was also found in a previous study reviewed by Barthès et al. (2008) that examined 18 topsoils in low-activity clay soils and

demonstrated that the TOC proportions in the > 200, 200–20 and < 20 μm fractions were 8, 17 and 65%, respectively. These results illustrate that different size fractions have different effects on SOC distributions. This study also showed that among the three different couplet types, TOC was positively correlated with SOC amount in each microaggregate fraction, especially the fine fraction. Consequently, changes in the TOC result from changes in different size fractions but depend more heavily on those fine fractions. This finding is also in agreement with the results of a study conducted by Barthès et al. (2008) that showed that TOC is especially positively correlated with the < 20 μm fraction. Roscoe et al. (2001) also found positive correlations between the TOC and SOC amounts for a clayey Oxisol under bush savannah and pasture conditions. Moreover, the SOC concentrations in the 50–20 and 250–50 μm fractions are positively correlated with one another but negatively correlated with that in the < 20 μm fraction. This pattern is mainly due to the different organic components among the microaggregate fractions. Several previous works support the conclusion that the organic constituents of the > 20 μm fraction mainly include plant debris and that these components are less decomposed and exhibit more recognizable morphologies in the coarser fractions than in the finer fractions. However, the organic components in the < 20 μm fraction are more humified and present a slower turnover time (Baldock and Skjemstad, 2000; Feller and Beare, 1997; Guggenberger and Haider, 2002).

The 250–50 μm fraction has the highest mean SOC concentration, primarily because fine microaggregates are bound together into larger ones by transient (i.e., microbial- and plant-derived polysaccharides) and temporary (roots and fungal hyphae) binding agents (Six et al., 2000). The SOC concentrations of the three microaggregate fractions showed an inverse tendency related to the respective mass fraction which was mainly due to the dilution effects (Amelung et al., 1998). This finding may partly explain why the fine fraction (< 20 μm) had a high SOC concentration value, while the coarser ones (250–50 and 50–20 μm) had lower values in Couplet Type III.

The present study confirmed that the dominant controlling factor for SOC amount was SOC concentration in the coarse fractions (250–50 and 50–20 μm) and the mass fraction in the fine fraction (< 20 μm). These results are partly inconsistent with those of a study conducted by Cambardella and Elliott (1993), which showed that the main controlling factor of SOC amount is the mass fraction rather than the SOC concentration for all aggregate fractions (> 2000, 2000–250, 250–53 and < 53 μm) in cultivated and grassland soils. This difference is mainly attributable to the different soil textures of the study areas examined (Barthès et al., 2008). Meanwhile, particle enrichment can be expected to result in SOC enrichment. Couplet Type I had the highest mean amount of SOC among the three couplet types primarily because fine particles are associated with a larger surface area, which is conducive to retaining/binding organic matter (Palis et al., 1997; Zinn et al., 2007).

4.3. Effects of soil erosion on the distribution and deposition of microaggregate SOC

Soil erosion and deposition induced by erosive rainstorms facilitates

the modification of aggregate size distributions and associated organic carbon in aggregate fractions (Wang et al., 2014a). Our results confirmed that the diversity distributions of SOC in different couplet types were mainly related to the selectivity of different rainfall events. Erosion processes induced by different erosive forces may lead to different SOC concentrations in sediments through selective particle size mobilization. Indeed, an erosion process affecting only the topsoil should produce relatively high SOC concentrations (Owens et al., 2002), as seen for sheet and interrill erosion (Schiettecatte et al., 2008). For non-selective erosion processes, such as rill and gully erosion, lower SOC concentrations are expected because SOC-rich topsoil is mixed with deeper SOC-poor horizons (Schiettecatte et al., 2008). In our study, we found that the average SOC concentrations of Couplet Types I, II and III were 2.61, 1.89 and 1.57 g kg⁻¹, respectively. However, regardless of whether selective or non-selective erosion processes are involved, the mobilized material is affected by the preferential transport of fine silt- and clay sized particles detached from the source soil (Starr et al., 2000). This observation is consistent with our findings that the 50–20 and < 20 µm fractions have higher mass fraction values than the 250–50 µm fraction. Furthermore, the 50–20 and < 20 µm microaggregate fractions contribute 77.5% of the TOC and play an important role in carbon sequestration in this check dam.

In the Loess Plateau gully region, organic carbon transport and storage are essentially linked to the differently sized fractions arising from erosive rainfall events (Wang et al., 2014c). During these events, large sediments loads can be transported from upper slopes to lower-elevation regions. When the precipitation level is high, large volumes of water flow towards rills and gullies, and rill and gully erosion gradually increase (Shi and Shao, 2000; Xu et al., 2004). In the context of such rapid transport, the eroded C has little opportunity to decompose during transport, and a significant fraction of the C is delivered to depositional areas (Berhe et al., 2007). Consequently, the high C storage levels in check dam deposits are attributed to the large volume of sediments generated by rill and gully erosion.

5. Conclusions

In this study, we explored the effects of different erosion processes on the SOC dynamics of microaggregate fractions in the check dam-controlled Nianyangou catchment on the Loess Plateau based on aggregate size distributions and rainfall events. The microaggregate fractions and associated SOC distributions were closely related to either sheet and interrill erosion or rill and gully erosion. Sediments with fine microaggregate fractions (Couplet Type I) had the highest amount of SOC and were most likely related to sheet and interrill erosion, whereas sediments with coarse microaggregate fractions (Couplet Type III) had the highest SOC concentration and were related to rill and gully erosion. Our results indicate that two main typical erosion processes affect the microaggregate fractions and the related SOC mobilization and deposition in this intensively cultivated catchment. Rill and gully erosion are the dominant erosion processes affecting the abundance SOC in the check dam.

The examined check dam serves as a carbon storage and sequestration structure, and its soil erosion-derived sediments could serve as an important indicator of environmental change. The advantages of investigating environmental changes based on sediments collected from check dams include the higher time resolution of the reconstructed information. Additionally, the check dams on the Loess Plateau feature broad temporal and spatial distributions, and approximately 80% of the SOC in the sediments trapped by check dams are present within the 50–20 and < 20 µm microaggregate fractions, representing a physically protected form of SOC. Consequently, check dams appear to play a key role in environmental protection by mitigating greenhouse gas emissions by storing large volumes of well-protected sedimentary organic carbon.

Acknowledgements

The financial support of the National Natural Science Foundation of China (Grant Nos. 41571130082, 41671281, and 41071194) and the Major Programs of the Chinese Academy of Sciences (KZZD-EW-04-03) for the work reported in this paper are gratefully acknowledged.

References

- Amelung, W., Zech, W., Zhang, X., Follett, R.F., Tiessen, H., Knox, E., Flach, K.W., 1998. Carbon, nitrogen, and sulfur pools in particle-size fractions as influenced by climate. *Soil Sci. Soc. Am. J.* 62, 172–181. <http://dx.doi.org/10.2136/sssaj1998.03615995006200010023x>.
- Anderberg, M.R., 1988. *Cluster Analysis for Applications*. Academic, New York.
- Baldock, J.A., Skjemstad, J.O., 2000. Role of the soil matrix and minerals in protecting natural organic materials against biological attack. *Org. Geochem.* 31, 697–710. [http://dx.doi.org/10.1016/S0146-6380\(00\)00049-8](http://dx.doi.org/10.1016/S0146-6380(00)00049-8).
- Barreto, R.C., Madari, B.E., Maddock, J.E.L., Machado, P.L.O.A., Torres, E., Franchini, J., Costa, A.R., 2009. The impact of soil management on aggregation, carbon stabilization and carbon loss as CO₂ in the surface layer of a rhodic Ferralsol in Southern Brazil. *Agr. Ecosyst. Environ.* 132, 243–251. <http://dx.doi.org/10.1016/j.agee.2009.04.008>.
- Barthès, B.G., Kouakoua, E., Larré-Larrouy, M., Razafimbelo, T.M., de Luca, E.F., Azontonde, A., Neves, C.S.V.J., de Freitas, P.L., Feller, C.L., 2008. Texture and sesquioxide effects on water-stable aggregates and organic matter in some tropical soils. *Geoderma* 143, 14–25. <http://dx.doi.org/10.1016/j.geoderma.2007.10.003>.
- Berhe, A.A., Harte, J., Harden, J.W., Torn, M.S., 2007. The significance of the erosion-induced terrestrial carbon sink. *Bioscience* 57, 337–346. <http://dx.doi.org/10.1641/B570408>.
- Beuselinck, L., Steegen, A., Govers, G., Nachtergaele, J., Takken, I., Poesen, J., 2000. Characteristics of sediment deposits formed by intense rainfall events in small catchments in the Belgian loam belt. *Geomorphology* 32, 69–82. [http://dx.doi.org/10.1016/S0169-555X\(99\)00068-9](http://dx.doi.org/10.1016/S0169-555X(99)00068-9).
- Cambardella, C.A., Elliott, E.T., 1993. Carbon and nitrogen distribution in aggregates from cultivated and native grassland soils. *Soil Sci. Soc. Am. J.* 57, 1071–1076. <http://dx.doi.org/10.2136/sssaj1993.03615995005700040032x>.
- Cao, S., Chen, L., Yu, X., 2009. Impact of China's Grain for Green Project on the landscape of vulnerable arid and semi-arid agricultural regions: a case study in northern Shaanxi Province. *J. Appl. Ecol.* 46, 536–543. <http://dx.doi.org/10.1111/j.1365-2664.2008.01605.x>.
- Cao, S., Wang, G., Chen, L., 2010. Questionable value of planting thirsty trees in dry regions. *Nature* 465, 31. <http://dx.doi.org/10.1038/465031d>.
- Chen, F., Fang, N., Shi, Z., 2016. Using biomarkers as fingerprint properties to identify sediment sources in a small catchment. *Sci. Total Environ.* 557–558, 123–133. <http://dx.doi.org/10.1016/j.scitotenv.2016.03.028>.
- Collins, A.L., Walling, D.E., Leeks, G.J.L., 1997. Fingerprinting the origin of fluvial suspended sediment in larger river basins: combining assessment of spatial provenance and source type. *Geografiska Annaler A* 79, 239–254. <http://dx.doi.org/10.1111/j.0435-3676.1997.00020.x>.
- Dearing, J., Hu, Y., Doody, P., James, P.A., Brauer, A., 2001. Preliminary reconstruction of sediment-source linkages for the past 6000 yr at the Petit Lac d'Annecy, France, based on mineral magnetic data. *J. Paleolimnol.* 25, 245–258. <http://dx.doi.org/10.1023/A:1008186501993>.
- Dearing, J.A., Jones, R.T., Shen, J., Yang, X., Boyle, J.F., Foster, G.C., Croom, D.S., Elvin, M.J.D., 2008. Using multiple archives to understand past and present climate-human-environment interactions: the lake Erhai catchment, Yunnan Province, China. *J. Paleolimnol.* 40, 3–31. <http://dx.doi.org/10.1007/s10933-007-9182-2>.
- Durnford, D., King, J.P., 1993. Experimental study of processes and particle-size distributions of eroded soil. *J. Irrig. Drain. Eng.* 119, 383–398. [http://dx.doi.org/10.1061/\(ASCE\)0733-9437\(1993\)119:2\(383\)](http://dx.doi.org/10.1061/(ASCE)0733-9437(1993)119:2(383)).
- Fang, N., Shi, Z., Li, L., Guo, Z., Liu, Q., Ai, L., 2012. The effects of rainfall regimes and land use changes on runoff and soil loss in a small mountainous watershed. *Catena* 99, 1–8. <http://dx.doi.org/10.1016/j.catena.2012.07.004>.
- Feller, C., Beare, M.H., 1997. Physical control of soil organic matter dynamics in the tropics. *Geoderma* 79, 69–116. [http://dx.doi.org/10.1016/S0016-7061\(97\)00039-6](http://dx.doi.org/10.1016/S0016-7061(97)00039-6).
- Fu, B., Chen, L., Ma, K., Zhou, H., Wang, J., 2000. The relationships between land use and soil conditions in the hilly area of the loess plateau in northern Shaanxi, China. *Catena* 39, 69–78. [http://dx.doi.org/10.1016/S0341-8162\(99\)00084-3](http://dx.doi.org/10.1016/S0341-8162(99)00084-3).
- Fu, X., Shao, M., Wei, X., Horton, R., 2010. Soil organic carbon and total nitrogen as affected by vegetation types in Northern Loess Plateau of China. *Geoderma* 155, 31–35. <http://dx.doi.org/10.1016/j.geoderma.2009.11.020>.
- Fu, B., Liu, Y., Lü, Y., He, C., Zeng, Y., Wu, B., 2011. Assessing the soil erosion control service of ecosystems change in the Loess Plateau of China. *Ecol. Complex.* 8, 284–293. <http://dx.doi.org/10.1016/j.ecocom.2011.07.003>.
- Girardclos, S., Fiore, J., Rachoud-Schneider, A., Baster, I., Wildi, W., 2005. Petit-Lac (western Lake Geneva) environment and climate history from deglaciation to the present: a synthesis. *Boreas* 34, 417–433. <http://dx.doi.org/10.1080/03099480500231385>.
- Golchin, A., Clarke, P., Oades, J., Skjemstad, J., 1995. The effects of cultivation on the composition of organic-matter and structural stability of soils. *Aust. J. Soil Res.* 33, 975–993. <http://dx.doi.org/10.1071/SR950975>.
- Gregorich, E.G., Greer, K.J., Anderson, D.W., Liang, B.C., 1998. Carbon distribution and losses: erosion and deposition effects. *Soil Till. Res.* 47, 291–302. <http://dx.doi.org/>

- 10.1016/S0167-1987(98)00117-2.
- Guggenberger, G., Haider, K.M., 2002. Effect of mineral colloids on biogeochemical cycling of C, N, P, and S in soil. In: Huang, P.M., Bollag, J.M., Senesi, N. (Eds.), *Interactions Between Soil Particles and Microorganisms, Impact on the Terrestrial Ecosystem*. Wiley and Sons, Chichester, pp. 267–322.
- Harden, J.W., Sharpe, J.M., Parton, W.J., Ojima, D.S., Fries, T.L., Huntington, T.G., Dabney, S.M., 1999. Dynamic replacement and loss of soil carbon on eroding cropland. *Global Biogeochem. Cycles* 13, 885–901. <http://dx.doi.org/10.1029/1999GB900061>.
- Products and Servicing Solution Teaching Book for SPSS of Windows Statistical. In: Hong, N. (Ed.), Tsinghua University Press, and Beijing Communication University Press Beijing, pp. 300–311 (in Chinese with English abstract).
- Issa, O.M., Bissonnais, Y.L., Planchon, O., Favis-Mortlock, D., Silvera, N., Wainwright, J., 2006. Soil detachment and transport on field-and laboratory-scale interrill areas: erosion processes and the size-selectivity of eroded sediment. *Earth Surf. Process. Landforms* 31, 929–939. <http://dx.doi.org/10.1002/esp.1303>.
- Jennings, A.E., Hagen, S., HarDardóttir, J., Stein, R., Ogilvie, A.E.J., Jónsdóttir, I., 2001. Oceanographic change and terrestrial human impacts in a post ad 1400 sediment record from the southwest Iceland shelf. *Clim. Change* 48, 83–100. <http://dx.doi.org/10.1023/A:1005658620319>.
- Klaminder, J., Appleby, P., Crook, P., Renberg, I., 2012. Post-deposition diffusion of ¹³⁷Cs in lake sediment: implications for radiocesium dating. *Sedimentology* 59, 2259–2267. <http://dx.doi.org/10.1111/j.1365-3091.2012.01343.x>.
- Lü, Y., Sun, R., Fu, B., Wang, Y., 2012. Carbon retention by check dams: regional scale estimation. *Ecol. Eng.* 44, 139–146. <http://dx.doi.org/10.1016/j.ecoleng.2012.03.020>.
- Lafren, J.M., Tian, J., 2000. *Soil Erosion and Dryland Farming*. Soil Erosion and Dryland Farming. CRC Press, Boca Raton, FL.
- Lal, R., 2003. Soil erosion and the global carbon budget. *Environ. Int.* 29, 437–450. [http://dx.doi.org/10.1016/S0160-4120\(02\)00192-7](http://dx.doi.org/10.1016/S0160-4120(02)00192-7).
- Liu, G.S., Jiang, N.H., Zhang, L.D., Liu, Z.L., 1996. *Soil Physical and Chemical Analysis and Description of Soil Profiles* (In Chinese) 24. China Standard Methods Presspp. 266.
- Nadeu, E., de Vente, J., Martínez-Mena, M., Boix-Fayos, C., 2011. Exploring particle size distribution and organic carbon pools mobilized by different erosion processes at the catchment scale. *J. Soils Sediments* 11, 667–678. <http://dx.doi.org/10.1007/s11368-011-0348-1>.
- Owens, L.B., Malone, R.W., Hothem, D.L., Starr, G.C., Lal, R., 2002. Sediment carbon concentration and transport from small watersheds under various conservation tillage practices. *Soil Till. Res.* 67, 65–73. [http://dx.doi.org/10.1016/S0167-1987\(02\)00031-4](http://dx.doi.org/10.1016/S0167-1987(02)00031-4).
- Palis, R., Okwach, G., Rose, C., Saffigna, P., 1990. Soil erosion processes and nutrient loss. I. The interpretation of enrichment ratio and nitrogen loss in runoff sediment. *Aust. J. Soil Res.* 28, 623–639. <http://dx.doi.org/10.1071/SR9900623>.
- Palis, R.G., Ghandiri, H., Rose, C.W., Saffigna, P.G., 1997. Soil erosion and nutrient loss. III. Changes in the enrichment ratio of total nitrogen and organic carbon under rainfall detachment and entrainment. *Aust. J. Soil Res.* 35, 891–905. <http://dx.doi.org/10.1071/S92060>.
- Panuska, J.C., Karthikeyan, K.G., Miller, P.S., 2008. Impact of surface roughness and crusting on particle size distribution of edge-of-field sediments. *Geoderma* 145, 315–324. <http://dx.doi.org/10.1016/j.geoderma.2008.03.015>.
- Peng, T., Wang, S., 2012. Effects of land use, land cover and rainfall regimes on the surface runoff and soil loss on karst slopes in southwest China. *Catena* 90, 53–62. <http://dx.doi.org/10.1016/j.catena.2011.11.001>.
- Perruchet, C., 1983. Constrained agglomerative hierarchical classification. *Pattern Recognit.* 16, 213–217. [http://dx.doi.org/10.1016/0031-3203\(83\)90024-9](http://dx.doi.org/10.1016/0031-3203(83)90024-9).
- Razafimbelo, T.M., Albrecht, A., Oliver, R., Chevallier, T., Chapuis-Lardy, L., Feller, C., 2008. Aggregate associated-C and physical protection in a tropical clayey soil under Malagasy conventional and no-tillage systems. *Soil Till. Res.* 98, 140–149. <http://dx.doi.org/10.1016/j.still.2007.10.012>.
- Ritchie, J.C., McHenry, J.R., 1990. Application of radioactive fallout cesium-137 for measuring soil erosion and sediment accumulation rates and patterns: a review. *J. Environ. Qual.* 19, 215–233. <http://dx.doi.org/10.2134/jeq1990.00472425001900020006x>.
- Roscoe, R., Buurman, P., Velthorst, E.J., Vasconcellos, C.A., 2001. Soil organic matter dynamics in density and particle size fractions as revealed by the ¹³C/¹²C isotopic ratio in a Cerrado's oxisol. *Geoderma* 104, 185–202. [http://dx.doi.org/10.1016/S0016-7061\(01\)00080-5](http://dx.doi.org/10.1016/S0016-7061(01)00080-5).
- Rose, C.W., Yu, B., Ghadiri, H., Asadi, H., Parlange, J.Y., Hogarth, W.L., Hussein, J., 2007. Dynamic erosion of soil in steady sheet flow. *J. Hydrol.* 333, 449–458. <http://dx.doi.org/10.1016/j.jhydrol.2006.09.016>.
- Salomé, C., Nunan, N., Pouteau, V., Lerch, T.Z., Chenu, C., 2010. Carbon dynamics in topsoil and in subsoil may be controlled by different regulatory mechanisms. *Glob. Change Biol.* 16, 416–426. <http://dx.doi.org/10.1111/j.1365-2486.2009.01884.x>.
- Saviozzi, A., Riffaldi, R., Levi-Minzi, R., Panichi, A., 1997. Properties of soil particle size separates after 40 years of continuous corn. *Commun. Soil Sci. Plant Anal.* 28, 427–440. <http://dx.doi.org/10.1080/00103629709369801>.
- Schietecatte, W., Gabriels, D., Cornelis, W.M., Hofman, G., 2008. Enrichment of organic carbon in sediment transport by interrill and rill erosion processes. *Soil Sci. Soc. Am. J.* 72, 50–55. <http://dx.doi.org/10.2136/sssaj2007.0201>.
- Shi, H., Shao, M., 2000. Soil and water loss from the Loess Plateau in China. *J. Arid Environ.* 45, 9–20. <http://dx.doi.org/10.1006/jare.1999.0618>.
- Shi, Z.H., Fang, N.F., Wu, F.Z., Wang, L., Yue, B.J., Wu, G.L., 2012. Soil erosion processes and sediment sorting associated with transport mechanisms on steep slopes. *J. Hydrol.* 454–455, 123–130. <http://dx.doi.org/10.1016/j.jhydrol.2012.06.004>.
- Shi, Z.H., Yue, B.J., Wang, L., Fang, N.F., Wang, D., Wu, F.Z., 2013. Effects of mulch cover rate on interrill erosion processes and the size selectivity of eroded sediment on steep slopes. *Soil Sci. Soc. Am. J.* 77, 257–267. <http://dx.doi.org/10.2136/sssaj2012.0273>.
- Six, J., Paustian, K., Elliott, E.T., Combrink, C., 2000. Soil structure and organic matter I: Distribution of aggregate-size classes and aggregate-associated carbon. *Soil Sci. Soc. Am. J.* 64, 681–689.
- Six, J., Bossuyt, H., Degryze, S., Denef, K., 2004. A history of research on the link between (micro) aggregates, soil biota, and soil organic matter dynamics. *Soil Till. Res.* 79, 7–31. <http://dx.doi.org/10.1016/j.still.2004.03.008>.
- Slattery, M.C., Burt, T.P., 1997. Particle size characteristics of suspended sediment in hillslope runoff and stream flow. *Earth Surf. Process Landforms* 22, 705–719.
- Smith, P., Fang, C., Dawson, J.J.C., Moncrieff, J.B., 2008. Impact of global warming on soil organic carbon. *Adv. Agron.* 97, 1–43. [http://dx.doi.org/10.1016/S0065-2113\(07\)00001-6](http://dx.doi.org/10.1016/S0065-2113(07)00001-6).
- Sritrairat, S., Peteet, D.M., Kenna, T.C., Sambrotto, R., Kurdyla, D., Guilderson, T., 2012. A history of vegetation, sediment and nutrient dynamics at Tivoli North Bay, Hudson estuary, New York. *Estuar. Coast. Shelf Sci.* 102–103, 24–35. <http://dx.doi.org/10.1016/j.ecss.2012.03.003>.
- Stallard, R.F., 1998. Terrestrial sedimentation and the carbon cycle: coupling weathering and erosion to carbon burial. *Global Biogeochem. Cycles* 12, 231–257. <http://dx.doi.org/10.1029/98GB00741>.
- Starr, G.C., Lal, R., Malone, R., Hothem, D., Owens, L., Kimble, J., 2000. Modeling soil carbon transported by water erosion processes. *Land Degrad. Dev.* 11, 83–91. [http://dx.doi.org/10.1002/\(SICI\)1099-145X\(200001/02\)11:1<83::AID-LDR370>3.0.CO;2-W](http://dx.doi.org/10.1002/(SICI)1099-145X(200001/02)11:1<83::AID-LDR370>3.0.CO;2-W).
- Stemmer, M., Gerzabek, M.H., Kandeler, E., 1998. Organic matter and enzyme activity in particle-size fractions of soils obtained after low-energy sonication. *Soil Biol. Biochem.* 30, 9–17. [http://dx.doi.org/10.1016/S0038-0717\(97\)00093-X](http://dx.doi.org/10.1016/S0038-0717(97)00093-X).
- Van Oost, K., Quine, T.A., Govers, G., De Gryze, S., Six, J., Harden, J.W., Ritchie, J.C., McCarty, G.W., Heckrath, G., Kosmas, C., Giraldez, J.V., da Silva, J.R., Merckx, R., 2007. The impact of agricultural soil erosion on the global carbon cycle. *Science* 318, 626–629. <http://dx.doi.org/10.1126/science.1145724>.
- Walling, D.E., He, Q., 1997. Use of fallout ¹³⁷Cs in investigations of overbank sediment deposition on river floodplains. *Catena* 29, 263–282. [http://dx.doi.org/10.1016/S0341-8162\(96\)00072-0](http://dx.doi.org/10.1016/S0341-8162(96)00072-0).
- Wang, Y.F., Fu, B.J., Chen, L.D., Lü, Y.H., Gao, Y., 2011. Check dam in the Loess Plateau of China: engineering for environmental services and food security. *Environ. Sci. Technol.* 45, 10298–10299.
- Wang, X., Cammeraat, E.L.H., Cerli, C., Kalbitz, K., 2014a. Soil aggregation and the stabilization of organic carbon as affected by erosion and deposition. *Soil Biol. Biochem.* 72, 55–65. <http://dx.doi.org/10.1016/j.soilbio.2014.01.018>.
- Wang, Y., Chen, L., Fu, B., Lü, Y., 2014b. Check dam sediments: an important indicator of the effects of environmental changes on soil erosion in the Loess Plateau in China. *Environ. Monit. Assess.* 186, 4275–4287. <http://dx.doi.org/10.1007/s10661-014-3697-6>.
- Wang, Y., Chen, L., Gao, Y., Wang, S., Lü, Y., Fu, B., 2014c. Carbon sequestration function of check-dams: a case study of the Loess Plateau in China. *Ambio* 43, 926–931. <http://dx.doi.org/10.1007/s13280-014-0518-7>.
- Wasson, R.J., Caitcheon, G., Murray, A.S., McCulloch, M., Quade, J., 2002. Sourcing sediment using multiple tracers in the catchment of lake argyle, Northwestern Australia. *Environ. Manage.* 29, 634–646. <http://dx.doi.org/10.1007/s00267-001-0049-4>.
- Xie, Y., Liu, B.Y., Zhang, W.B., 2000. Study on standard of erosive rainfall. *J. Soils Water Conserv.* 14, 6–11 (in Chinese with English abstract).
- Xu, X.Z., Zhang, H.W., Zhang, O.Y., 2004. Development of check-dam systems in gullies on the Loess Plateau. *China. Environ. Sci. Policy* 7, 79–86. <http://dx.doi.org/10.1016/j.envsci.2003.12.002>.
- Xue, K., Yang, M.Y., Zhang, F.B., Sun, X.J., 2011. Investigating soil erosion history of a small watershed using sediment couplet in a dam. *J. Nucl. Agric. Sci.* 25 (1), 115–120 (in Chinese with English abstract).
- Yang, M., Tian, J., Liu, P., 2006. Investigating the spatial distribution of soil erosion and deposition in a small catchment on the Loess Plateau of China, using ¹³⁷Cs. *Soil Till. Res.* 87, 186–193. <http://dx.doi.org/10.1016/j.still.2005.03.010>.
- Yang, X.H., Jia, Z.Q., Ci, L.J., 2010. Assessing effects of afforestation projects in China. *Nature* 466, 315.
- Yeh, H.-Y., Wensel, L.C., Turnblom, E.C., 2000. An objective approach for classifying precipitation patterns to study climatic effects on tree growth. *For. Ecol. Manag.* 139, 41–50. [http://dx.doi.org/10.1016/S0378-1127\(99\)00332-1](http://dx.doi.org/10.1016/S0378-1127(99)00332-1).
- Zhang, X., Walling, D.E., Yang, Q., He, X., Wen, Z., Qi, Y., Feng, M., 2006. ¹³⁷Cs budget during the period of 1960 in a small drainage basin on the Loess Plateau of China. *J. Environ. Radioact.* 86, 78–91. <http://dx.doi.org/10.1016/j.jenvrad.2005.07.007>.
- Zhao, G., Klik, A., Mu, X., Wang, F., Gao, P., Sun, W., 2015. Sediment yield estimation in a small watershed on the northern Loess Plateau, China. *Geomorphology* 241, 343–352. <http://dx.doi.org/10.1016/j.geomorph.2015.04.020>.
- Zinn, Y.L., Lal, R., Bigham, J.M., Resck, D.V.S., 2007. Eddy controls on soil organic carbon retention in the Brazilian Cerrado: texture and mineralogy. *Soil Sci. Soc. Am. J.* 71, 1204–1214. <http://dx.doi.org/10.2136/sssaj2006.0014>.